https://doi.org/10.5194/egusphere-2026-1261
Preprint. Discussion started: 18 March 2026

Bottom currents at the Arctic Mid Oceanic Ridge: insights from deployed sensors, biological indicators, and global models

Alban Souche[1], Camilla M. Marnor[1], Ebbe H. Hartz[2], Anders Tengberg[3], and Daniel W. Schmid[1]

[1]Bergverk AS, Sandefjord, Norway
[2]Aker BP ASA, Lysaker, Norway
[3]Aanderaa Data Instruments AS, Bergen, Norway

Correspondence: Alban Souche (alban.souche@bergwerk.com)

Abstract. Characterizing near-bottom ocean currents at deep-sea topographic features requires observations across multiple scales, from basin-wide circulation models to local in situ measurements. This study addresses this challenge at DeepInsight Hill on the Mohns Ridge by combining eight months of in situ current measurements, global ocean model predictions, and novel ROV-based biological flow indicators. Our findings reveal a complex and highly variable flow regime with a striking decoupling between tidal pressure and near-bottom currents. Spectral analysis shows that the dominant semi-diurnal tidal pressure signal does not translate into coherent near-bottom currents, suggesting conversion of tidal energy into internal waves at the ridge topography. During winter, sustained directional transport occurs simultaneously in opposite directions at the summit and base of DeepInsight Hill (S-SE and N-NW respectively), accounting for most of the effective water displacement over the record. However, foliaceous sponges, whose fan-shaped morphology is known to develop perpendicular to the prevailing current, show consistent W-SW orientations at the base of the hill that do not match the long-term instrumental mean flow direction (N-NW). Instead, these orientations align with global model predictions and the direction of episodic peak currents recorded during summer, suggesting that sponge morphology records specific high-energy flow events rather than time-averaged conditions, possibly amplified by peak summer nutrient supply. Bedforms observed at the same location eight months apart show no significant change, indicating that sediment-mobilizing currents are episodic and may not recur annually. Further data and interdisciplinary research are essential to resolve the governing factors of these systems and to refine environmental impact assessments in topographically complex deep-sea settings.

1 Introduction

Understanding seafoor ocean currents in the deep sea is essential for benthic habitat characterization, environmental impact assessment, and operational planning of deep-sea activities. Flow regimes control sediment transport, nutrient delivery, larval dispersal, and the dispersal of sediment plumes, all critical factors for benthic communities and for evaluating the environmental consequences of deep-sea resource exploration. Seamounts and topographic highs are known to generate complex hydrodynamic regimes through interactions between currents, tides, and topography, with important consequences for benthic communities (Lavelle and Mohn, 2010). Yet integrating observations across multiple scales, from basin-wide circulation spanning hundreds of kilometers to local biological indicators at meter scales, remains a significant challenge.

https://doi.org/10.5194/egusphere-2026-1261
Preprint. Discussion started: 18 March 2026

Near-bottom current measurements at deep-sea topographic features remain scarce, yet recent studies have revealed surprisingly complex and energetic flow regimes. At the Schulz Bank seamount on the Arctic Mid-Ocean Ridge, Roberts et al. (2018) characterized the oceanographic setting and short-timescale variability, and Hanz et al. (2021) deployed a benthic lander for one year and documented current speeds with daily fluctuations of about 0.4 m s^{-1} around a mean of 0.14 m s^{-1}, with peaks reaching 0.72 m s^{-1} during winter. Their spectral analysis showed that semi-diurnal and diurnal tidal constituents dominated the current signal, and that internal waves generated by tidal flow over the seamount topography enhanced turbulent mixing and nutrient supply to the summit sponge ground. Within the New England Seamounts, Godin et al. (2024) reported strong near-bottom currents at even greater depths (~2500-4400m depth), with maximum speeds exceeding 1.10 m s^{-1}. The influence of seabed morphology on near-bottom currents has been documented across diverse settings. Using moorings stations over four years periods offshore Mozambique, Bailey et al. (2024) shows that submarine canyons and gullies strongly steer and funnel flows in ways that differ substantially from regional circulation patterns. Frey et al. (2025) provides a detailed mapping and analysis of bedforms over a volcanic seamount in the Kermadec arc, showing that bottom currents vary spatially at scales of meters to hundreds of meters and fluctuate on daily timescales, with currents reaching up to 1 m s^{-1}. These studies collectively highlight that near-bottom flow conditions at topographic features are poorly predicted by regional-scale models and require in situ characterization.

DeepInsight Hill is located on the Mohns Ridge in the Norwegian-Greenland Sea, adjacent to the active mid-ocean ridge volcanic axis (Figure 1). The hill forms a circular dome approximately 5 km in diameter with an elevation of about 1000 m from base to summit, and a total vertical difference of about 2000 m from the deepest part of the volcanic central axis 15 km to the south-east. The age of the oceanic crust at this location is estimated at 3 to 4 Ma (Gaina, 2014). The geological origin remains uncertain but its dome morphology and position relative to the spreading axis are compatible with an oceanic core complex structure (Blackman et al., 2009). Structural ridges aligned in oblique N-NE to S-SW directions along the northern and southern margins create elongated valleys. The region hosts several extinct seafloor massive sulfide (eSMS) deposits, including the DeepInsight and Grøntua deposits (Voje et al., 2025), whose discovery triggered substantial scientific interest and motivated several research expeditions within the EMINENT program beginning in 2023 (Aarrestad et al., 2024; Voje et al., 2025).

In terms of ocean circulation, DeepInsight Hill lies at the boundary of two large basin cyclonic gyres (Bosse et al., 2019; Voet et al., 2010). The regional patterns are illustrated in Figure 1 (b), showing flow vectors from the Copernicus global model for 2024 at the seafloor (Copernicus Marine Service, 2024). Mean flow vectors reveal predominantly south-west flow in the southern part of DeepInsight Hill and north-east oriented flow in the northern part. The north-eastward flow reflects the Greenland Basin Gyre circulation, while the south-westward current shows a more complex relationship with the Lofoten Basin Gyre, as the Mohns Ridge acts as a mixing zone between these two major circulation systems (Bosse et al., 2019; Voet et al., 2010).

The complex topography of DeepInsight Hill, combined with diverse benthic communities including deep-sea sponge aggregations whose distribution is linked to oceanographic processes (Davison et al., 2019), makes this site well suited for investigating the interaction between physical oceanographic processes and biological systems. This study addresses this by combining in

https://doi.org/10.5194/egusphere-2026-1261
Preprint. Discussion started: 18 March 2026

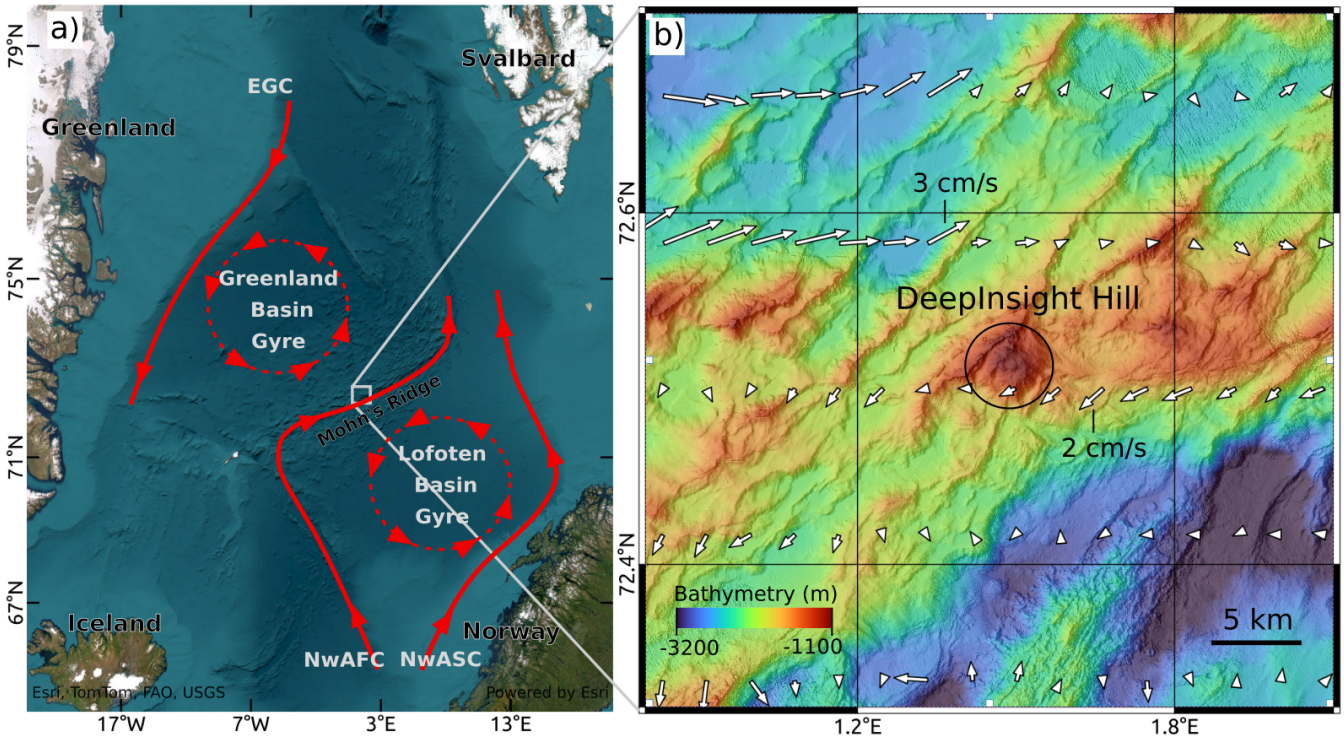

Figure 1. Regional and local circulation patterns. (a) Large-scale map showing the DeepInsight Hill region along Mohn's Ridge segment of the Arctic Mid Oceanic Ridge. The figure illustrates the main regional surface current patterns with the Lofoten Basin and the Greenland Basin Gyres, the East Greenland Current (EGC), the Norwegian Atlantic Slope and Front Current (NwASC and NwAFC) (Bosse et al., 2019; Voet et al., 2010). Bathymetry basemap sources: Esri, TomTom, FAO, USGS | Powered by Esri. (b) Detailed view of the study area with mean bottom flow vectors from the 2024 Copernicus model with annotated flow amplitude for scale. Bathymetry from -3200 to -1100 meters shown in color scale.

situ current measurements from multi-month current meter deployments, biological flow indicators identified from ROV video surveys, and predictions from the Copernicus global ocean model. The objectives are to: (1) characterize ocean currents using these complementary approaches, (2) compare global-scale model predictions with local measurements and biological indicators, and (3) demonstrate the utility of biological flow indicators for understanding prevailing and instantaneous flow conditions.

2 Methods

Data collection efforts around DeepInsight Hill included four research expeditions conducted over three years (2023-2025), extensive ROV video footage from multiple dives, flow sensors at the seafloor collecting current data, and bathymetry mapping (Aarrestad et al., 2024, Voje et al. (2025)).

https://doi.org/10.5194/egusphere-2026-1261
Preprint. Discussion started: 18 March 2026

2.1 Copernicus Global Scale Ocean Models

We used the Copernicus Global Ocean Physics Analysis and Forecast model (Copernicus Marine Service, 2024) to extract three-dimensional ocean current data for the year 2024. This global model provides historical ocean state estimates and forecasts over the past two years at any location and depth, with a spatial resolution suitable for analyzing regional-scale circulation patterns. The model has a horizontal resolution of 0.083° in both longitude and latitude, corresponding in our study area to approximately 2.8 km and 9.2 km, respectively, and includes 50 vertical layers representing water depths from the surface to about 5500 m. At the depths relevant to our study area (from approximately 1000 m at the top of the hill to 2000 m at the base), the model layers are discretized at approximately 100-meter vertical resolution. To characterize average flow conditions, we computed the annual mean current field for 2024 by averaging the monthly datasets, and selected the model layer closest to the seafloor at each grid point to approximate near-seafloor current conditions.

2.2 In Situ Current Measurements

Two multiparameter current meters (SeaGuard-1322 and SeaGuard-1338 from Aanderaa-Xylem, Figure 2) were deployed at the seafloor for approximately 8 months during 2023-2024. Each instrument was equipped with a single-point Doppler current sensor measuring horizontal currents approximately 0.5 m above the seafloor at 0.25 Hz. An averaged current vector was recoded at 10-minute intervals from 150 measurments. The stations were positioned in the upper and lower sections of DeepInsight Hill, separated by approximately 2.5 km, and measured current velocity, direction, pressure, suspended particles, and other oceanographic parameters not presented in this work (e.g. temperature, oxygen, salinity, and turbidity) (Figure 2). Notably, the stations deployed at the base of the hill are located within an elongated valley oriented along the main W-SW structural trend, which may locally channel and amplify currents measured at these positions.

Additional deployments during the February 2025 EMINENT excursion included short-term deployments lasting several days at multiple locations during the cruise survey (Figure 2), with a higher recording rate of one-minute intervals. These instruments were deployed and recovered by ROV during short dive operations.

2.3 Benthic Flow Indicators

ROV videos were analyzed from the EMINENT excursions from 2023 to 2025 at multiple dive sites covering different depth ranges and seafloor types. Two categories of biological flow indicators were identified and analyzed:

Instantaneous flow indicators included soft benthic tissues, such as tunicates, that align with current direction, and fish observed orienting against current. These indicators reflect current conditions at the time of observation.

Morphological flow indicators included foliaceous sponges whose growth morphology reflects prevailing flow conditions over longer time scales. These sponges develop vertically fan-like forms oriented perpendicular to the current with their concave side facing upstream (Schönberg, 2021). However, as discussed below, the interpretation of these indicators is not straightforward and their alignment may reflect the strongest current events rather than time-averaged flow conditions.

https://doi.org/10.5194/egusphere-2026-1261
Preprint. Discussion started: 18 March 2026

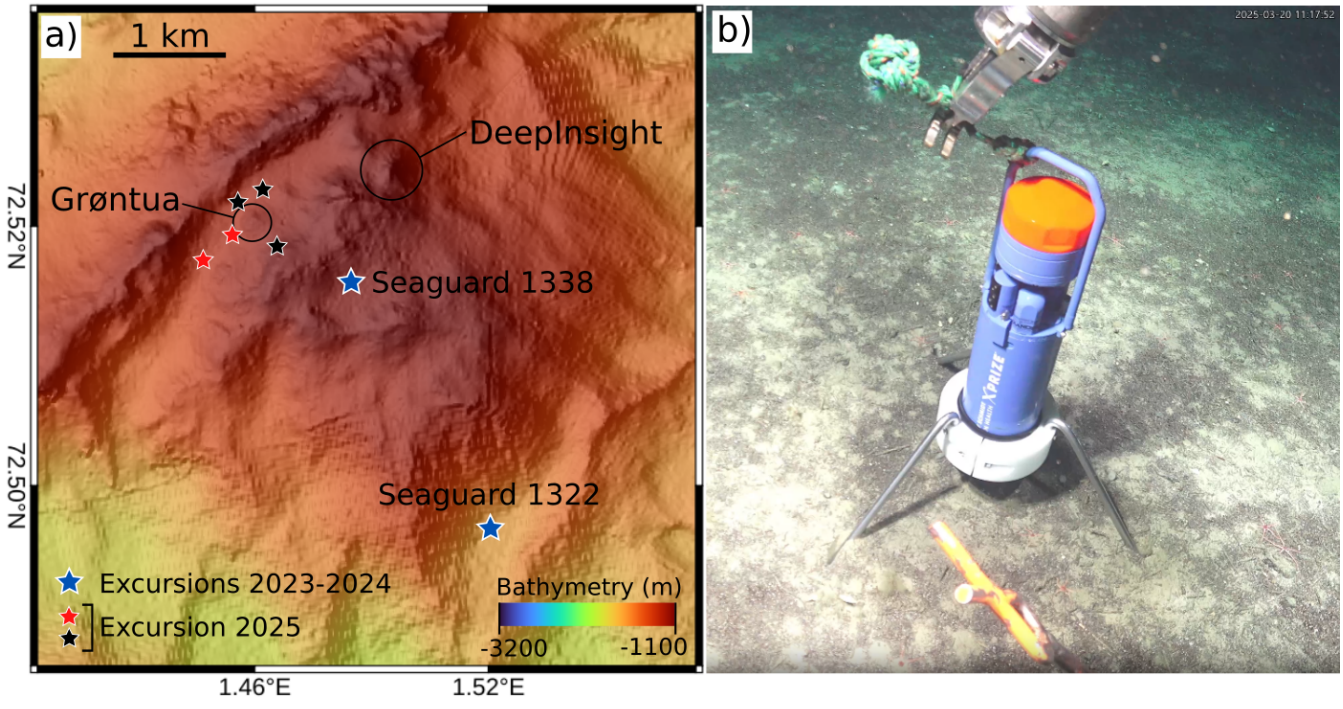

Figure 2. SeaGuard deployment locations. (a) Map of the DeepInsight Hill area showing the locations of DeepInsight and Grøntua sulfide deposit hills, and the deployment positions of SeaGuard current meters during the 2023-2024 and 2025 EMINENT research expeditions. (b) ROV photograph showing a SeaGuard current meter on the seafloor being retrieved by the ROV manipulator arm. The orange sensor on the top is measuring currents, particles and instrument tilt every 4 s at approximately 0.5 m above the seafloor. Below is a suite of sensors that provide information on pressure, temperature, salinity, turbidity and oxygen.

Bedforms in sediments are commonly seen over the area. These features may indicate prevailing currents, but their formation timescales and persistence are not yet well understood. Bedforms may form during episodic strong current events and remain on the seafloor until subsequent events. While we document the presence of bedforms in this work, they were not included as morphological flow indicators in the dataset presented in Figure 3.

3 Results

3.1 Benthic Flow Indicators

The spatial distribution of benthic flow indicators reveals a clear segregation between morphological and instantaneous indicators that correlates with topographic position (Figure 3). At the base of the hill, morphological flow indicators are abundant and show remarkably consistent W-SW orientations, in good agreement with the global-scale model predictions (Figure 3 (a)). By contrast, the top of the hill shows very few morphological flow indicators, and those present display a N or E trend. Instanta-

https://doi.org/10.5194/egusphere-2026-1261
Preprint. Discussion started: 18 March 2026

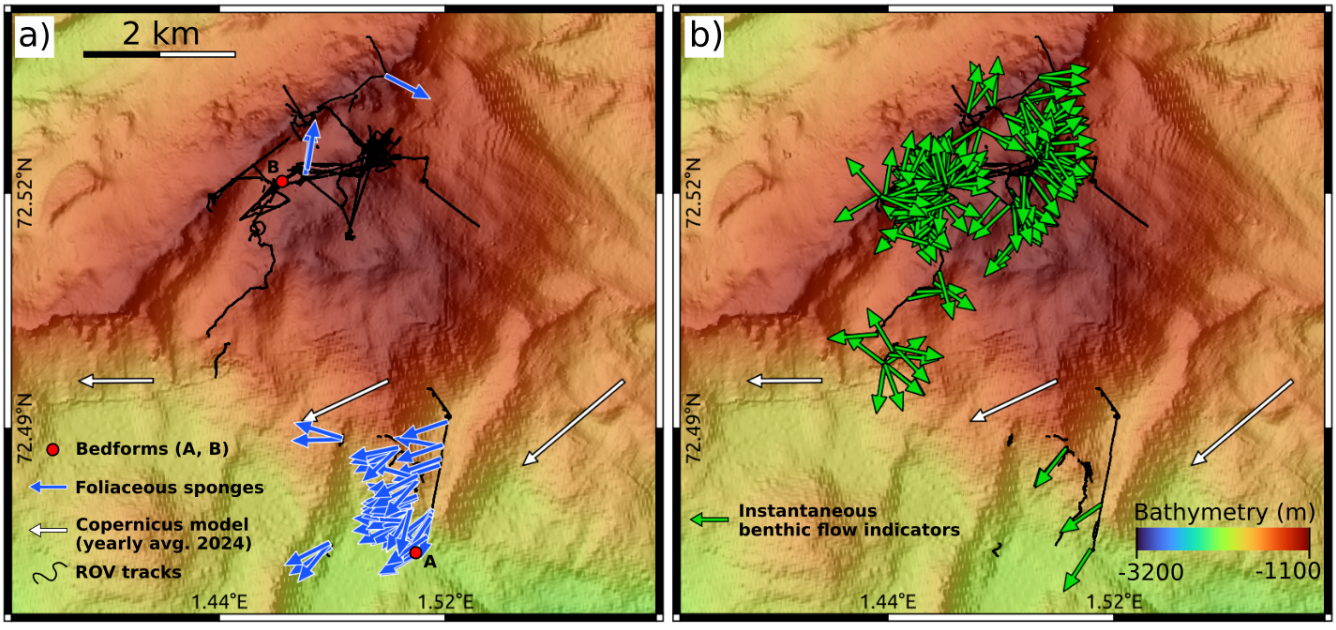

Figure 3. Spatial distribution of benthic flow indicators and comparison with Copernicus model predictions. (a) Map showing morphological flow indicators (foliaceous sponges) observed from ROV dives, with Copernicus model flow vectors (2024 mean), ROV survey tracks, and bathymetry. (b) Map showing instantaneous benthic flow indicators with the same background data.

neous flow indicators show concentration at the top of the hill (Figure 3 (b)) with highly fluctuating orientations, reflecting the temporal variability of flow conditions. The few instantaneous flow indicators observed at the base of the hill show orientations consistent with the morphological indicators in that area.

Figure 4 (a) presents a photogrammetry reconstruction of the seabed marked by different sand formations, with darker and lighter sediments showing distinct bedform patterns that are inferred to have formed orthogonal to the prevailing ocean current direction. Figure 4 (b) shows a detailed view of a stone with three foliaceous sponges that are morphologically shaped to face the flow, with their concave sides oriented into the current. These independent flow indicators are mutually consistent, both indicating W-SW flow in agreement with the year-average conditions predicted by the global-scale model.

Figure 5 illustrates examples of instantaneous flow indicators as identified from ROV video footage. Soft benthic tissues are visibly deflected by the ambient current, and their orientation is used to infer the instantaneous flow direction at the time of observation. The inferred directions are marked by arrows, which are then used to populate the instantaneous flow indicator dataset shown in Figure 3 (b).

https://doi.org/10.5194/egusphere-2026-1261
Preprint. Discussion started: 18 March 2026

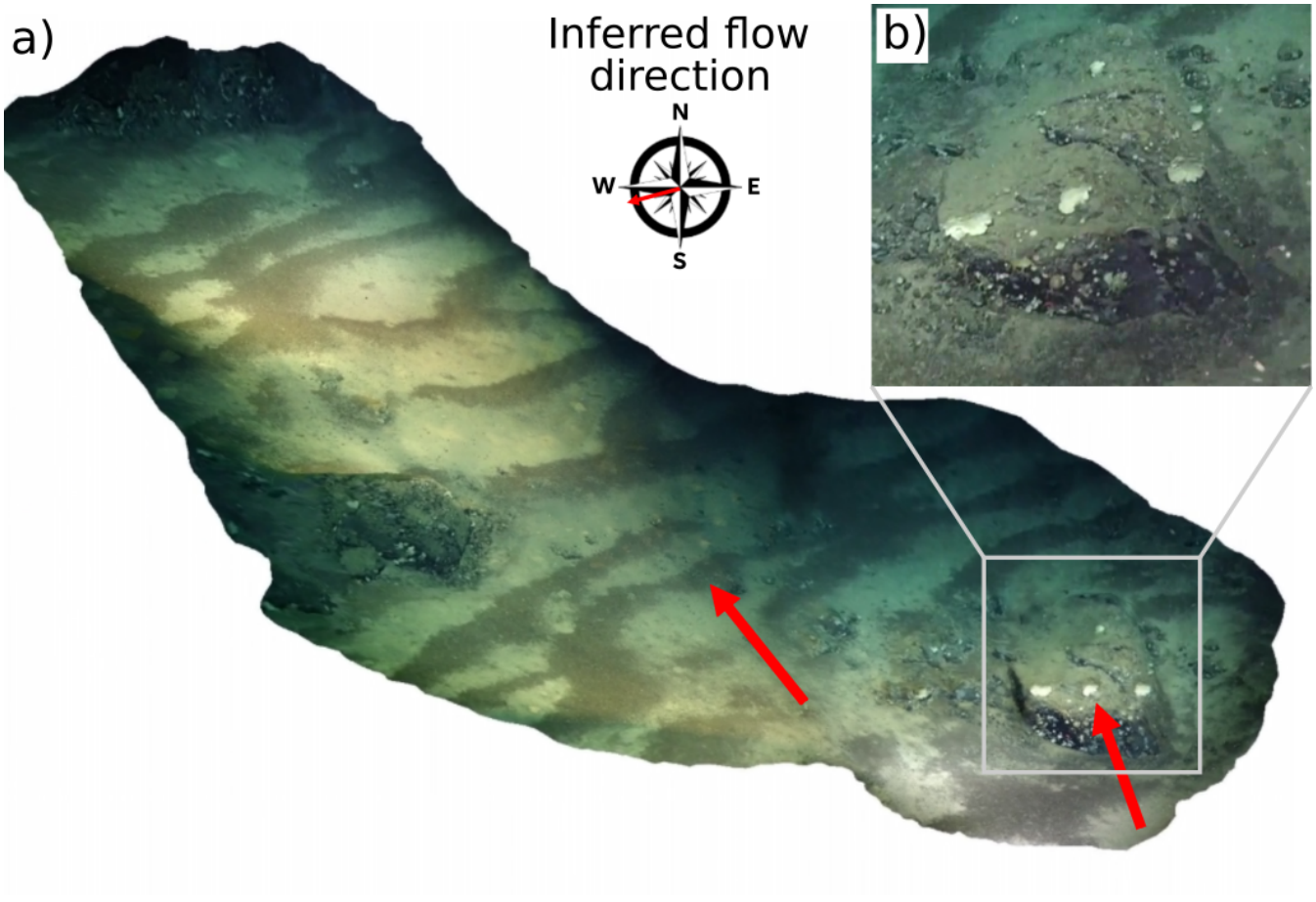

Figure 4. Prevailing flow indicators as current ripples and foliaceous sponges at the bedform localtion A (Figure 3 (a)). (a) Photogrammetry reconstruction of seabed marked by different sediment formations (dark and lighter) showing current ripple patterns inferred to have formed orthogonal to ocean current direction. (b) Zoom showing a stone with three foliaceous sponges morphologically shaped to face the flow. Video material from the dataset *2023-EMINENT-01*, see Data availability.

https://doi.org/10.5194/egusphere-2026-1261
Preprint. Discussion started: 18 March 2026

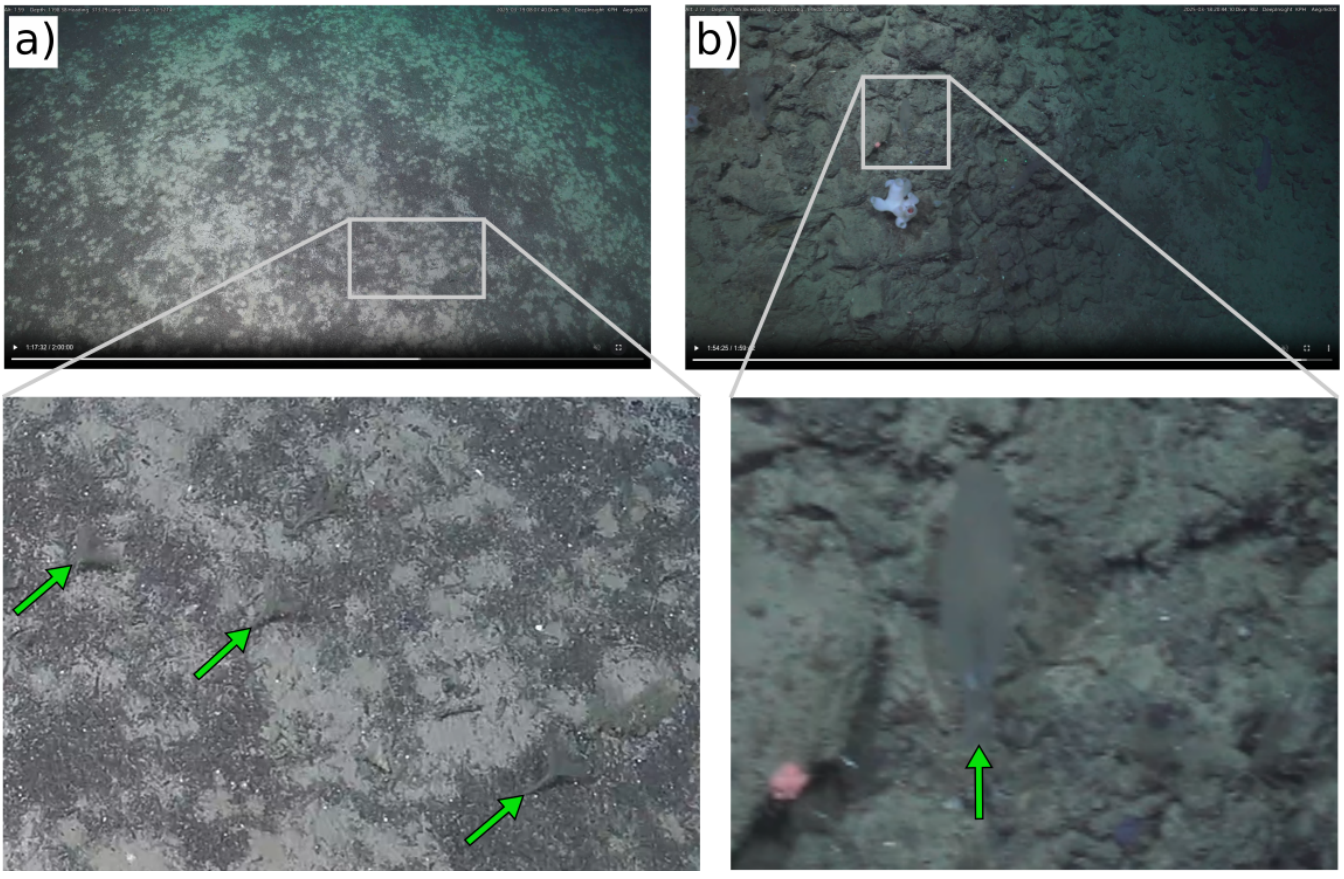

Figure 5. Examples of instantaneous benthic flow indicators observed in ROV video footage. Soft benthic tissues (tubeworms (a) and tunicates (b)) are visibly deflected by the ambient current. Green arrows indicate the inferred instantaneous flow direction based on tissue alignment.

3.2 In Situ Current Measurements

3.2.1 Spectral decomposition

SeaGuard 1322 and SeaGuard 1338 measurements were analyzed using spectral decomposition to identify periodic components in the current and pressure signals over the full 8-month deployment period (Figure 6). Panel (a) shows a representative 4-day time series from SeaGuard 1322, where the pressure signal exhibits a clear 12-hour cyclic pattern corresponding to semi-diurnal tides. However, this 12-hour periodicity is not reflected in the absolute speed or direction of the current signals. Panel (b) presents the power spectral density analysis of the full 8-month record, confirming clear spectral peaks at 12 hours, 24 hours, and 14 days for the pressure signal. In contrast, the current speed and direction signals show peaks at 24 hours and 14 days, but the 12-hour peak is close to background fluctuation levels, indicating no clear expression of semi-diurnal tidal

https://doi.org/10.5194/egusphere-2026-1261
Preprint. Discussion started: 18 March 2026

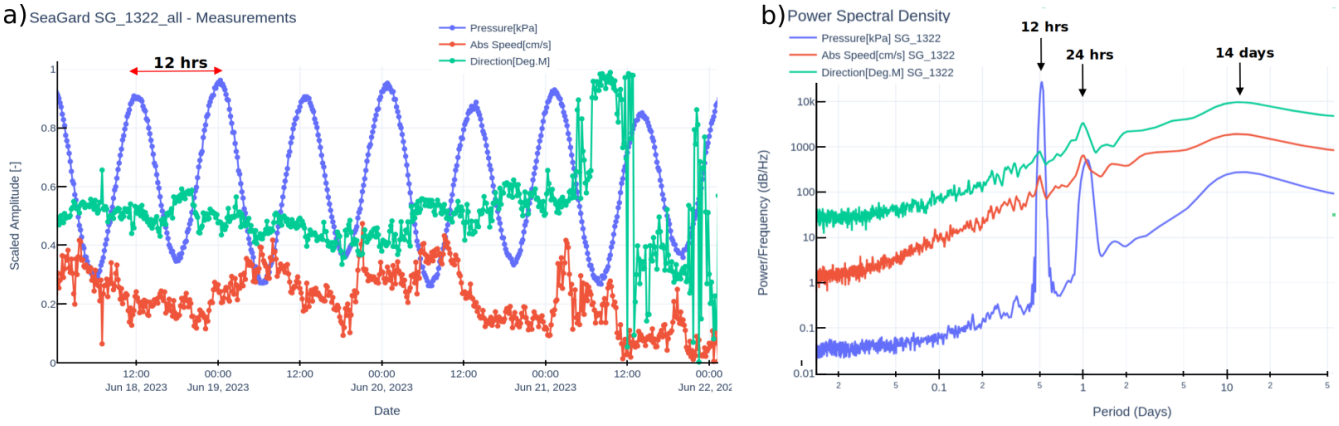

Figure 6. Spectral analysis of SeaGuard 1322 current and pressure data. (a) Time series example over 4 days showing cyclic pattern of 12 hours for the pressure signal, which is not reflected in the absolute speed or direction of the current signals. (b) Power spectral density of the full signal period (8 months) showing clear peaks at 12h, 24h, and 14 days for the pressure signal. The speed and direction signals show peaks at 24h and 14 days, but the 12h peak is close to background fluctuation with no clear expression of 12-hour cyclicity for these signals.

cyclicity in the flow patterns. Similar patterns are observed at SeaGuard 1338, suggesting that the semi-diurnal tidal forcing in pressure does not translate directly into semi-diurnal current variations at these locations.

3.2.2 Short-term variability

High-resolution measurements from the February 2025 deployments, sampled at one-minute intervals, captured detailed short-term variability across several tidal cycles (Figure 7). Panel (a) shows current speed color-coded by flow direction alongside the tidal pressure curve, revealing partial correlations between current behavior and the tidal signal at specific locations. In contrast, panel (b) demonstrates that this relationship is not systematic, showing no clear correspondence between tidal forcing and observed current patterns at that site. This spatial variability in tidal influence suggests that local topography and other forcing mechanisms may play important roles in modulating the flow regime on the semi-diurnal (12 h) timescale. This observation is consistent with the weak spectral energy identified at the 12 h period in the power spectrum analysis (Figure 6 (b)).

3.2.3 Long-term variability (2023-2024)

The fluctuations in current direction over the 8-month recording period are best understood by decomposing the signal over the 14-day lunar tidal cycle and sub-phases (Figure 8, Figure 9). The tidal pressure signals were divided into rising and falling phases of the lunar cycle using the upper envelope of the pressure time series.

Figure 8 presents data from SeaGuard 1338 located at the top of the study area. The current speed time series (Figure 8 (b)) shows highly fluctuating behavior with somewhat higher current trends in June 2023 and from November 2023 to January 2024. The backscatter signal (Figure 8 (c)) shows a marked increase in July, corresponding to the arrival at depth of spring bloom particles from increased surface biological activity in spring/summer, manifested as elevated particle concentrations in

https://doi.org/10.5194/egusphere-2026-1261
Preprint. Discussion started: 18 March 2026

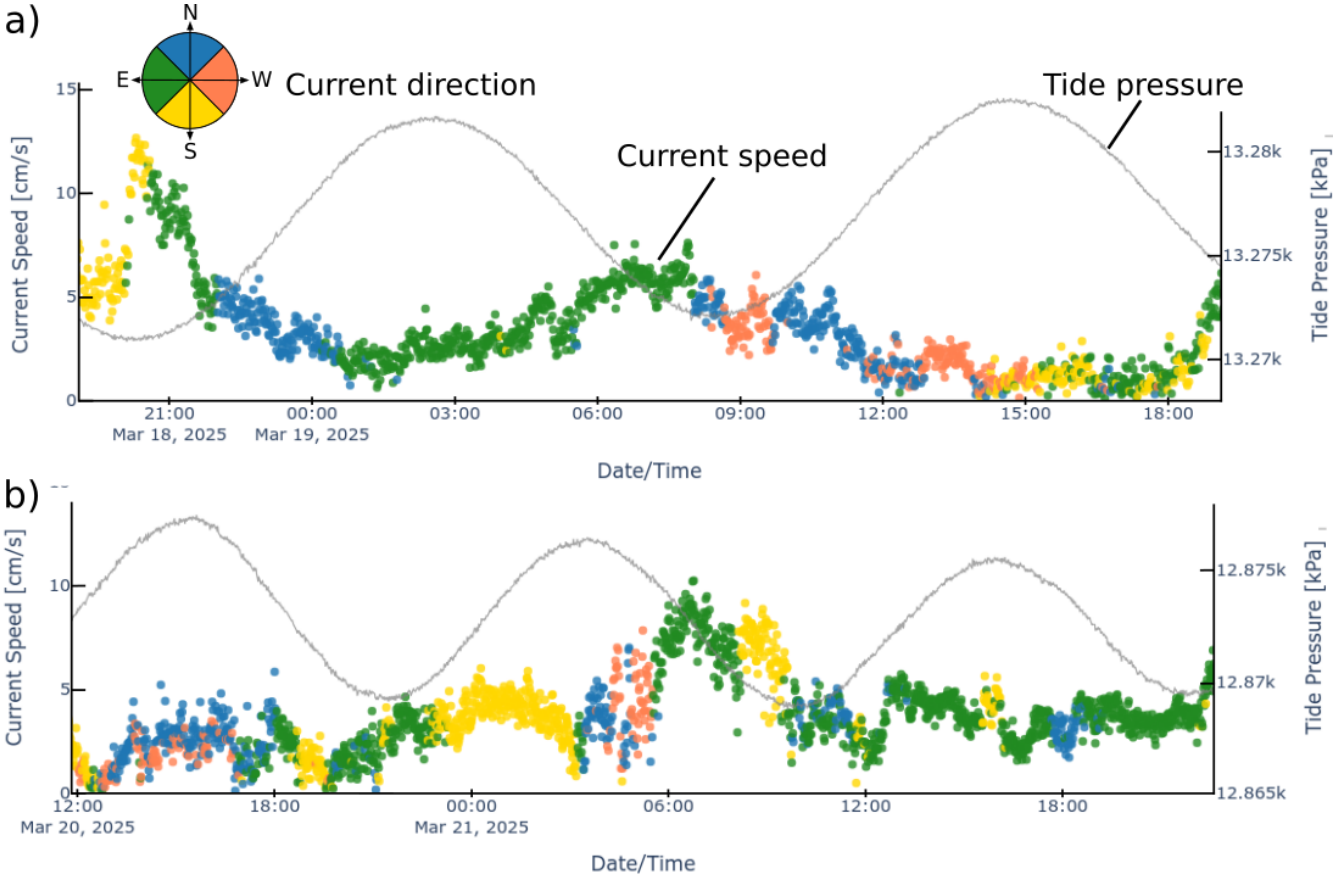

Figure 7. Time series of current measurements and tidal pressure over several tidal cycles from 2025 deployments. (a) Current speed (color-coded by flow direction) and tide pressure curve showing some correlation between current characteristics and tidal signal. (b) Current speed and tide pressure at a different location/time showing no clear correlation with tidal forcing.

the water column (marine snow). The progressive vector plot (Figure 8 (d)) reveals a relatively circular path characterized by fluctuating flow directions from May to November 2023, followed by a continuous south-eastward current from December 2023 to January 2024. The maximum current vectors for each rising and falling tide cycle (Figure 8 (e)) and their directional distribution (Figure 8 (f)) show that the main direction of strong flow components is oriented S-E. The mean flow vectors for each tide cycle (Figure 8 (g)) and their distribution (Figure 8 (h)) also reveal a dominant S-E direction of transport.

Figure 9 presents data from SeaGuard 1322 located at the base of the study area. Current speed and backscatter patterns show similar observations to SeaGuard 1338. The progressive vector plot (Figure 9 (d)) reveals a particularly dominant N-NW transport from November 2023 until January 2024. Before that period, the transport was highly fluctuating, forming loops. The maximum current vectors for each tide cycle (Figure 9 (e)) and their distribution (Figure 9 (f)) show an interesting main W-SW direction for the strongest flows, mostly represented from July to November 2023. These maximum flows are short-lived,

https://doi.org/10.5194/egusphere-2026-1261
Preprint. Discussion started: 18 March 2026

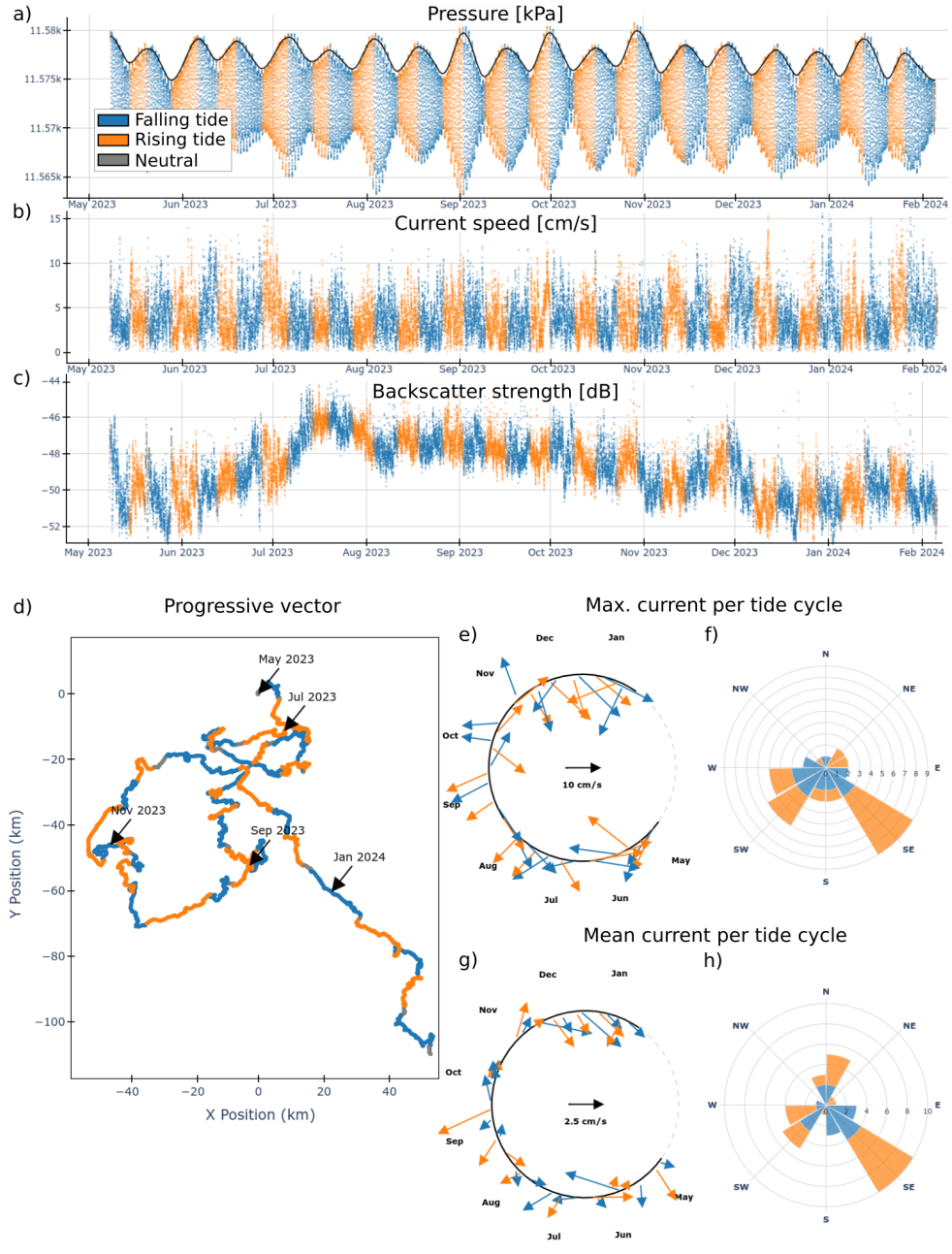

Figure 8. SeaGuard-1338 (top of the mount) current data from May 2023 to January 2024. (a) Tidal pressure time series with upper envelope used to define rising and falling lunar tide cycles (each point corresponds to a 10-minute average from the 15 Hz sensor). (b) Current speed time series (Max 16.0 cm/s; Average 4.0 cm/s). (c) Acoustic backscatter strength measuring water particle turbidity. (d) Progressive vector plot integrating current direction and speed over the recording period. (e) Maximum current vector for each tide cycle and (f) corresponding distribution of the current orientations. (g) Mean current vector for each tide cycle and (h) corresponding distribution of the current orientations.

https://doi.org/10.5194/egusphere-2026-1261
Preprint. Discussion started: 18 March 2026

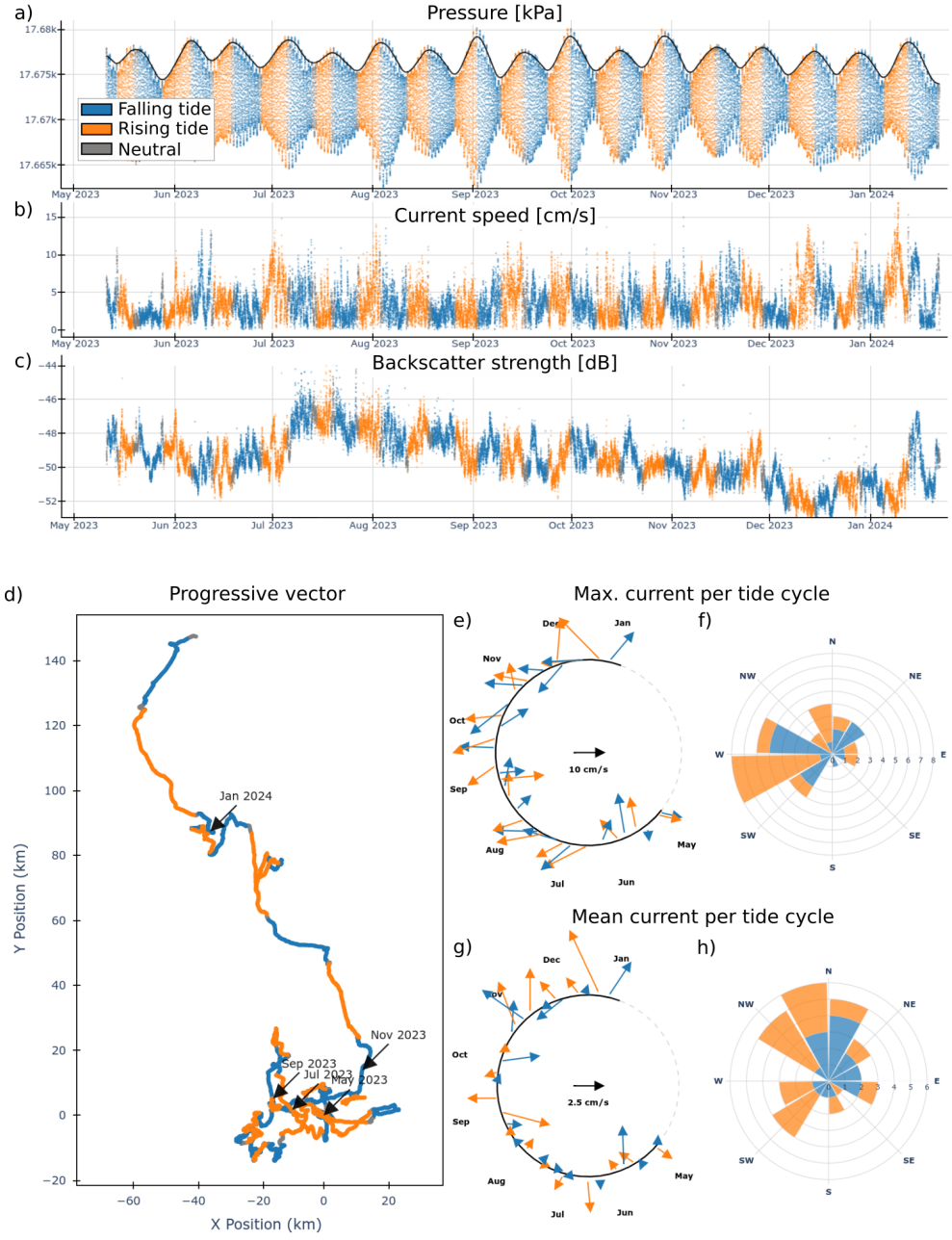

Figure 9. SeaGuard-1322 (base of the mount) current data from May 2023 to January 2024. (a) Tidal pressure time series with upper envelope used to define rising and falling lunar tide cycles (each point corresponds to a 10-minute average from the 15 Hz sensor). (b) Current speed time series (Max 17.7 cm/s; Average 3.7 cm/s). (c) Acoustic backscatter signal measuring water particle turbidity. (d) Progressive vector plot integrating current direction and speed over the recording period. (e) Maximum current vector for each tide cycle and (f) corresponding distribution of the current orientations. (g) Mean current vector for each tide cycle and (h) corresponding distribution of the current orientations.

https://doi.org/10.5194/egusphere-2026-1261
Preprint. Discussion started: 18 March 2026

and the averaged flow over each cycle (Figure 9 (g), Figure 9 (h)) shows a more N-NW trend. Notably, the maximum flow orientation (W-SW) corresponds to the main orientation of the foliaceous sponges and bedform morphological flow indicators observed at the base of the hill, while the mean flow direction (N-NW) does not.

3.3 Current Ripple Formation and Persistence

The observed bedforms (Figure 4) exhibit alignment patterns consistent with ripple formation under strong flow conditions, likely during short-lived, high-energy events. While the brighter material is clay sediment, the darker material may consist of agglutinated foraminifera, tube-like marine protists that construct their shells by selecting and cementing sedimentary grains (Linke and Lutze, 1993; Pearson and Party, 2018). Dense accumulations of these organisms and similar rod-like biogenic structures have been observed at other deep-sea locations such as Schulz Bank (Meyer et al., 2023). The potential difference in density and settling properties of these two materials may imply more complex sorting and transport dynamics than classical sand ripple formations.

A close comparison of ROV surveys performed at the same location near Grøntua in June 2024 and February 2025 revealed minimal change in the seabed formations (Figure 10 and Figure 11), indicating that these bedforms persist between episodes of strong flow. The absence of noticeable evolution over this approximately 8-month interval suggests that strong near-bed currents capable of bedform formation are episodic and may not recur every year.

4 Discussion

4.1 Benthic Flow Indicators: Interpretation and Limitations

4.1.1 Sponge Morphology Analysis

Following the framework of Schönberg (2021), sponge morphologies can be classified based on their functional relationship to flow conditions. Strong turbulent flow favors simple forms with large attachment areas, crusts, and simple-massive morphologies. Laminar flow conditions favor erect, vertically flattened, and flexible sponges that position themselves perpendicular to the current with their in-openings facing upstream. Where nutrient availability is limited, cup-like forms with separated inhalant and exhalant openings, as well as erect and stalked forms, tend to dominate.

At DeepInsight Hill, foliaceous sponges were found predominantly on rocky substrates in flat seafloor areas at the base of the hill, associated with sediment bedform patterns formed by current flow. This distribution is independently supported by Marnor et al. (2026), who mapped fan-shaped sponge counts across DeepInsight Hill using AI-assisted systematic analysis of ROV video footage. These sponges consistently showed W-SW orientations (approximately 260°), in good agreement with the Copernicus global model predictions. By contrast, the summit of DeepInsight Hill lacks sponges displaying characteristic foliaceous morphology. Culwick et al. (2020) showed that sponge density and distribution in the deep sea are constrained by fluid forcing, with local hydrodynamic conditions determining where sponges can establish and persist. The absence of foliaceous sponges at the summit could indicate more variable flow conditions in this area, with no clear prevailing orientation.

https://doi.org/10.5194/egusphere-2026-1261
Preprint. Discussion started: 18 March 2026

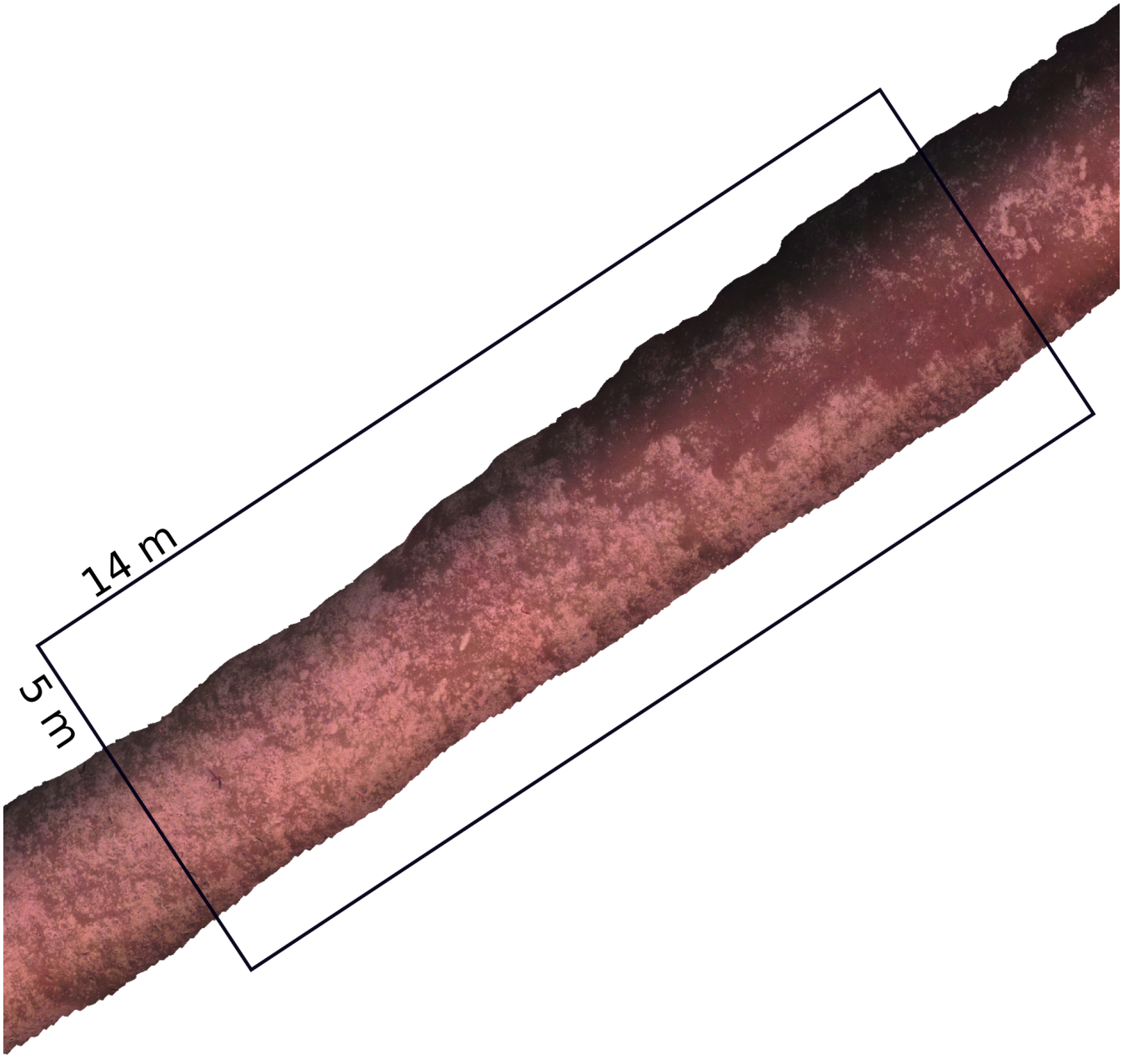

Figure 10. Sediment pattern at the bedform location B (Figure 3 (a)) in June 2024. Photogrammetry reconstructed section of the ROV dive940 (20240629-201442) from CDeepSea2024 excursion (UiB).

https://doi.org/10.5194/egusphere-2026-1261
Preprint. Discussion started: 18 March 2026

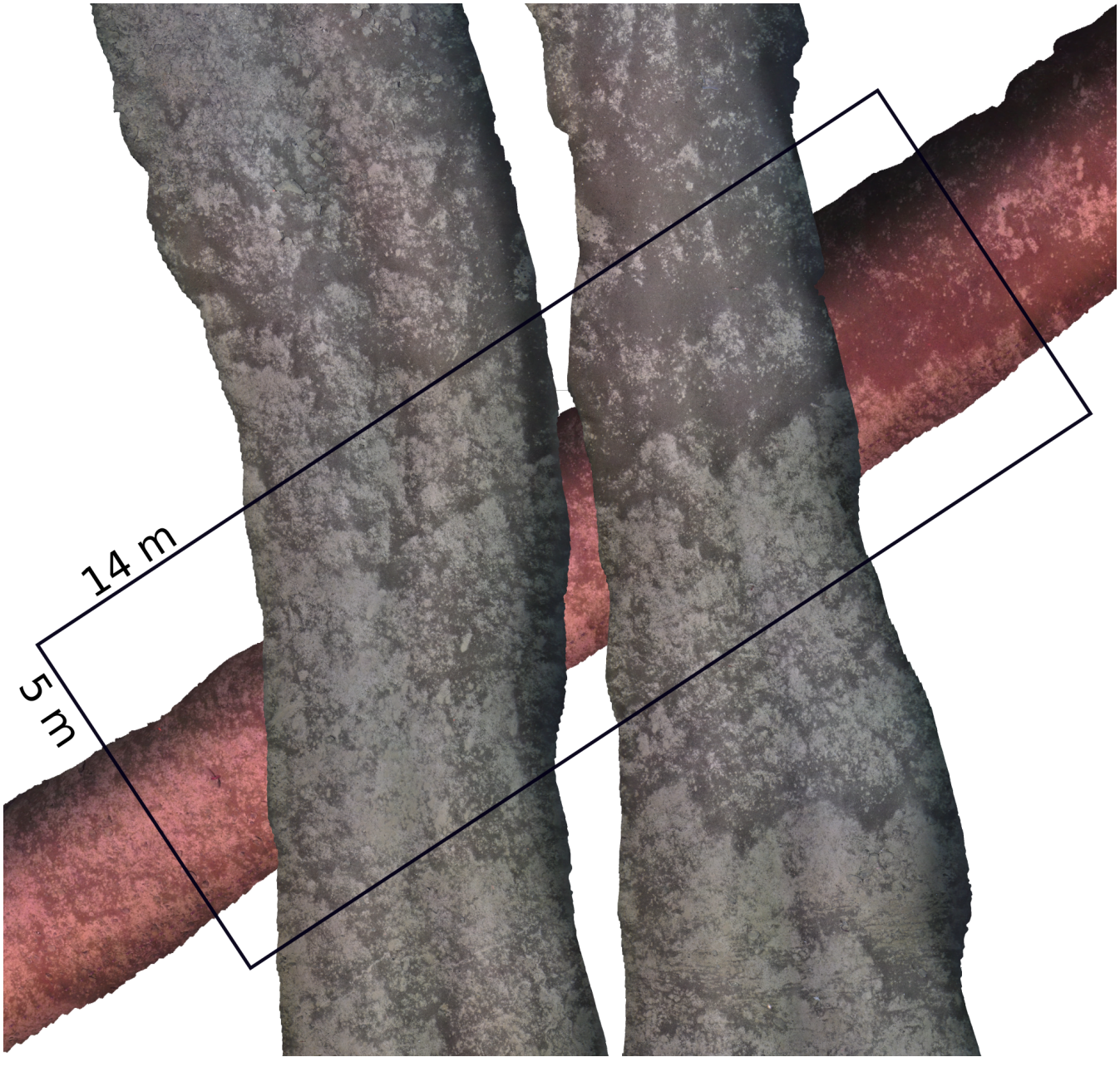

Figure 11. Sediment pattern at the bedform location B (Figure 3 (a)) in February 2025 showing minimal change from (Figure 10). Photogrammetry reconstruction from ROV dive10 (20250320) from DeepInsight2025 excursion.

https://doi.org/10.5194/egusphere-2026-1261
Preprint. Discussion started: 18 March 2026

While the foliaceous sponge orientations align with the global model predictions, they do not correspond to the time-averaged mean flow direction recorded by the SeaGuard current meater. The SeaGuard 1322 data at the base of the hill provides key insights into this discrepancy. The maximum current vectors recorded from July to November 2023 show a dominant W-SW orientation (Figure 9 (e), Figure 9 (f)), matching the sponge and bedform orientations. However, these maximum flows are short-lived events, and the mean flow over each tidal cycle during this same period shows very little consistency in direction. This suggests that sponge morphology develops primarily in response to the strongest current events rather than to time-averaged flow conditions.

Notably, the July–November 2023 period during which the strongest W-SW currents were recorded also coincides with elevated particle concentrations in the water column (marine snow), raising the question of whether food supply timing also plays a role in sponge morphological development. This is discussed further below.

An important limitation is that the 8-month recording period (May 2023 to January 2024) does not cover a full annual cycle and may not be representative of the long-term flow conditions that shaped the sponge morphology over their lifespan. Longer time series of near seabed current and particle measurements will be needed to understand and model the governing factors.

4.1.2 Sediment Features as Flow Indicators

Ripples and bedforms record episodes of strong flow capable of mobilizing sediment, with their orientation indicating flow direction and their scale and shape reflecting flow velocity and sediment properties. A recent study by Frey et al. (2025) extensively mapped bedforms over the Havre Seamount in the Kermadec arc, revealing highly variable current conditions governed by topographic interactions at multiple scales. They demonstrated that bedform formation and reworking occur on timescales of hours to days during active current events, but that these features persist when flow conditions are quiescent. At DeepInsight Hill, bedform patterns observed at the same location in June 2024 and February 2025 show no noticeable change (Figure 10, Figure 11), indicating that bedform-forming currents did not occur during this interval. This suggests that such high-energy events are episodic and may not recur every year, and that the 8-month SeaGuard record likely captures typical rather than extreme flow conditions.

4.2 Tidal Dynamics and Near-Bottom Currents

The spectral analysis reveals a striking decoupling between tidal pressure and near-bottom currents at DeepInsight Hill. The pressure record shows clear energy peaks at 12 h, 24 h, and 14 days, but the 12-hour semi-diurnal peak is almost absent from the current speed and direction signals at both stations. The semi-diurnal tide, despite dominating the pressure signal, does not produce coherent horizontal currents at the seafloor. The 2025 short-term deployments confirm this observation where the high-resolution measurements (Figure 7) show that current behavior partially correlates with the tidal pressure signal at some locations but not systematically.

This behavior differs from what has been observed at other deep-sea topographic features. At the Schulz Bank seamount, Hanz et al. (2021) found that semi-diurnal and diurnal tidal constituents were the dominant components of the current signal, together contributing over 60% of the tidal energy. Similarly, van Haren et al. (2017) documented intense internal wave turbulence driven

https://doi.org/10.5194/egusphere-2026-1261
Preprint. Discussion started: 18 March 2026

by tidal forcing at a biologically rich Mid-Atlantic seamount, where tidal energy conversion over steep topography generated strong near-bottom currents in submarine canyons with clear tidal periodicity. At both sites, the interaction between tidal flow and topography translates into energetic and coherent near-bottom currents, the opposite of what is observed at DeepInsight Hill.

Several factors may explain this difference. First, DeepInsight Hill at 1000-2000 m depth on Mohn's Ridge lies at the boundary between the Greenland Basin and Lofoten Basin Gyres (Figure 1 (a)) (Bosse et al., 2019; Voet et al., 2010), creating an intermediate circulation zone where competing large-scale flows may weaken tidal current coherence. Second, the complex ridge topography may scatter tidal energy into incoherent internal waves rather than focusing it into coherent near-bottom currents (Lavelle and Mohn, 2010; Whalen et al., 2020; Mashayek et al., 2024; Souche et al., 2025).

The fortnightly (~14 day) lunar tidal cycle, by contrast, appears more clearly in the current records. The progressive vector plots (Figure 8 (d), Figure 9 (d)) suggest that transitions in transport direction may be associated with the rising and falling phases of the lunar tidal envelope. However, this relationship is qualitative and has not been formally tested. With only ~18 complete lunar cycles captured in the 8-month record, a rigorous statistical analysis is limited. Longer deployments would be needed to establish whether the fortnightly modulation of current direction is a robust feature of the flow regime at DeepInsight Hill.

4.3 Summit Versus Base Flow Regime

Current direction fluctuates significantly at both SeaGuard stations throughout the recording period. The progressive vector plots reveal two notable features. First, from May to November 2023, both stations show fluctuating directions and looping transport paths. From December 2023 to January 2024, both stations transition to sustained directional transport, but in opposite directions, S-SE at the summit (SeaGuard 1338) and N-NW at the base (SeaGuard 1322). This winter transport accounts for most of the effective water displacement at both stations over the 8-month record. Whether this shift reflects seasonal intensification of the large-scale gyre circulation or interannual variability cannot be determined from these data alone, as the record does not cover a full annual cycle. Notably, this winter intensification is consistent with observations at Schulz Bank, where Hanz et al. (2021) also recorded the strongest currents during winter.

The current amplitudes recorded at DeepInsight Hill are modest compared to other deep-sea topographic features. Mean current speeds at both SeaGuard stations are on the order of a few centimeters per second, with maximum speeds occasionally reaching approximately 0.20 m s^{-1}. These values are substantially lower than those reported at the nearby Schulz Bank, where mean speeds of 0.14 m s^{-1} and winter maximum speeds of 0.72 m s^{-1} were recorded at the summit (Hanz et al., 2021), and far below the extreme near-bottom currents exceeding 1.10 m s^{-1} measured at the New England Seamounts (Godin et al., 2024). At the Mozambique continental slope, Bailey et al. (2024) recorded near-bed current speeds typically between 0.2 and 0.4 m s^{-1}, with the fastest currents reaching up to 0.95 m s^{-1} in the upper sections of submarine canyons. The relatively weak currents at DeepInsight Hill likely reflect the absence of strong tidal amplification mechanisms at this location, as discussed above. It should also be noted that the above comparisons involve measurements taken at different heights above the seafloor, as instruments in the referenced studies were positioned at 3.5 m or higher, whereas ours measured at 0.5 m. Current speeds

https://doi.org/10.5194/egusphere-2026-1261
Preprint. Discussion started: 18 March 2026

decrease with proximity to the seabed within the bottom boundary layer, so these amplitude differences should be interpreted with some caution.

Along the southern margin of DeepInsight Hill, structural ridges oriented E-NE to W-SW form elongated valleys that may locally constrain and amplify currents. This topographic channeling could explain why the strongest currents at the base align with the W-SW structural trend. Bailey et al. (2024) demonstrated that such topographic steering of near-bed currents diminishes rapidly with distance from the seabed, being barely recognizable at 30 m above bottom in low-relief gullies. The proximity of the SeaGuard sensors to the seafloor (0.5 m above bottom) in our study therefore makes them well suited to capture these topographically channeled flows from the local ridges orientation.

4.4 Backscatter, Particle Flux, and Sponge Food Supply

The acoustic backscatter records at both stations show a marked increase beginning in July 2023, interpreted as the arrival at depth of spring bloom particles (marine snow) from enhanced surface biological productivity. A similar seasonal pattern was observed at Schulz Bank, where Hanz et al. (2021) reported an acoustic backscatter peak in September, slightly later than the July onset recorded at DeepInsight Hill. This difference may reflect inter-annual variability or the distinct latitudes of the two sites, but the overall behavior is comparable. Deep-sea sponges in the Norwegian-Greenland Sea depend on particle capture from the water column for their nutrition (Witte et al., 1997), and the seasonal sinking of spring bloom particles has been identified as a primary food supply mechanism for benthic communities at nearby seamounts (Hanz et al., 2021; Roberts et al., 2018). As noted previously, this period of elevated particle concentration at DeepInsight Hill also coincides with the interval during which the strongest W-SW currents were recorded at the base of the hill (July to November 2023). Whether this co-occurrence between peak food availability and maximum current events has biological significance remains an open question.

5 Conclusions

This study presents a multi-method framework for characterizing deep-sea ocean currents that integrates global ocean models, long-term in situ measurements, and novel ROV-based benthic biological flow indicators. Our findings reveal a complex and highly variable flow regime at DeepInsight Hill that would be impossible to resolve through a single data source alone. We have demonstrated that benthic organisms serve as proxies for different temporal scales of flow, with soft-tissue organisms like tunicates aligning with instantaneous current directions. By combining ROV-based biological flow indicators with traditional physical oceanography at the Arctic Mid-Oceanic Ridge, we have uncovered an apparent contradiction in sponge morphology: while the orientation of foliaceous sponges aligns with global models and episodic summer peaks, it does not reflect the long-term instrumental mean flow or the absolute winter maximums. This suggests that biological morphology may prioritize specific high-energy windows, potentially linked to seasonal nutrient flux such as marine snow. The integration of these data sources also highlights a striking pressure-current decoupling, where the dominant 12-hour semi-diurnal tidal pressure does not translate into coherent horizontal currents. Furthermore, the discovery of sustained winter transport occurring in opposite

https://doi.org/10.5194/egusphere-2026-1261
Preprint. Discussion started: 18 March 2026

directions (S-SE at the summit and N-NW at the base) highlights the influence of the boundary between the Greenland and Lofoten Basin Gyres. Despite these insights, this work emphasizes how much remains unknown. The stability of bedforms over an 8-month interval suggests that the high-energy events required for sediment transport are episodic and may not occur annually. Significant further research is required to determine the long-term recurrence intervals of these events and to resolve the physiological triggers that cause benthic communities to record specific flow orientations. Refining the integration of in situ biological data into high-resolution numerical models remains essential for more accurate Environmental Impact Assessments in topographically complex deep-sea settings.

Author contributions. Conceptualisation: AS, DWS, EHH; Data curration: AS, AT, and CMM; Investigation: AS; Visualisation: AS, DWS, EHH, AT; Original draft: AS; Reviewed and editing of the manuscript: AS, CMM, EHH, AT, DWS.

Competing interests. Authors AS, CM, and DS were employed by Bergverk AS, which received funding from Aker BP ASA. The funder, through their employee and co-author EH, was involved in the study conceptualization, visualization, review, and editing of the manuscript, as well as in the decision to submit the work for publication.

Data availability. The ROV video material *2024-NOD-02* and *2025-EMINENT-01* was obtained upon request from the Norwegian Offshore Directorate. The ROV video material *2023-EMINENT-01* was obtained upon request from the EMINENT project. The ROV video material *CDeepSea2024* was obtained upon request from the Center for Deep Sea Research, University of Bergen. The high-resolution bathymetry data corresponds to the MBES dataset *2024-NOD-01*, obtained from the Norwegian Offshore Directorate, and the publicly available digital elevation model from Geonorge (accessed on 10 March 2026). Global-scale ocean current data were retrieved from the Copernicus Marine Service (accessed on 10 March 2026). The current dataset from the Seaguards and the benthic indicators analyzed in this study can be made available from the corresponding author upon reasonable request.

Acknowledgements. This work was supported by AkerBP. We thank the EMINENT project, the University of Bergen (UiB), and the Norwegian Offshore Directorate (NOD) for data access. We are grateful to Ihne Håverstad Ousdal and Kari Haugo Skeie for their valuable contributions on the ROV-video analysis. We acknowledge the Copernicus Marine Environment Monitoring Service for providing global ocean model data. The authors used AI language model assistance to improve grammar and readability of the manuscript.

https://doi.org/10.5194/egusphere-2026-1261
Preprint. Discussion started: 18 March 2026

References

Aarrestad, I., Voje, T. J. T., Jæger, M. L., Wågbø, S. L., Kjemperud, A. O. J., Strand, T., Ousdal, I. H., Herskedal, S. S., Fredriksen, R., Thorseth, I. H., and Pedersen, R. B.: Mohns Ridge and Norwegian-Greenland Sea: Cruise Report, Cruise Report 2024-NOD-02, Center for Deep Sea Research, University of Bergen and Norwegian Offshore Directorate, Bergen, Norway, https://www.sodir.no/4ad7a2/globalassets/1-sodir/om-oss/opne-data/havbunnsmineraler-eng/2024-nod-02-report.pdf, cruise dates: 14.02.2024–02.03.2024, 2024.

Bailey, L. P., Clare, M. A., Hunt, J. E., Kane, I. A., Miramontes, E., Fonnesu, M., Argiolas, R., Malgesini, G., and Wallerand, R.: Highly variable deep-sea currents over tidal and seasonal timescales, Nature Geoscience, 17, 787–794, https://doi.org/10.1038/s41561-024-01494-2, 2024.

Blackman, D. K., Canales, J. P., and Harding, A.: Geophysical signatures of oceanic core complexes, Geophysical Journal International, 178, 593–613, https://doi.org/10.1111/j.1365-246X.2009.04184.x, 2009.

Bosse, A., Fer, I., Lilly, J. M., and Søiland, H.: Dynamical controls on the longevity of a non-linear vortex: The case of the Lofoten Basin Eddy, Scientific Reports, 9, 13 448, https://doi.org/10.1038/s41598-019-49599-8, 2019.

Copernicus Marine Service: Global Ocean Physics Analysis and Forecast, Copernicus Marine Environment Monitoring Service, https://doi.org/10.48670/moi-00016, 2024.

Culwick, T., Phillips, J., Sherwin, C., Mayfield, E. J., and Hendry, K. R.: Sponge density and distribution constrained by fluid forcing in the deep sea, Frontiers in Marine Science, 7, 395, https://doi.org/10.3389/fmars.2020.00395, 2020.

Davison, J. J., van Haren, H., Hosegood, P., Piechaud, N., and Howell, K. L.: The distribution of deep-sea sponge aggregations (Porifera) in relation to oceanographic processes in the Faroe-Shetland Channel, Deep Sea Research Part I: Oceanographic Research Papers, 146, 55–61, https://doi.org/10.1016/j.dsr.2019.03.005, 2019.

Frey, S. E., Jutzeler, M., Carey, R. J., and Harris, P. T.: In-situ sedimentary evidence of complex bottom currents at a modern deepwater seamount, Communications Earth & Environment, 6, 709, https://doi.org/10.1038/s43247-025-02690-7, 2025.

Gaina, C.: Age of Ocean Crust, https://doi.org/10.22008/FK2/KK5RQN, 2014.

Godin, O. A., Tan, T. W., Joseph, J. E., and Walters, M. W.: Observation of exceptionally strong near-bottom flows over the Atlantis II Seamounts in the northwest Atlantic, Scientific Reports, 14, 10 308, https://doi.org/10.1038/s41598-024-60528-2, 2024.

Hanz, U., Roberts, E. M., Duineveld, G., Davies, A., van Haren, H., Rapp, H. T., Reichart, G.-J., and Mienis, F.: Long-term Observations Reveal Environmental Conditions and Food Supply Mechanisms at an Arctic Deep-Sea Sponge Ground, Journal of Geophysical Research: Oceans, 126, e2020JC016 776, https://doi.org/10.1029/2020JC016776, 2021.

Lavelle, J. W. and Mohn, C.: Motion, commotion, and biophysical connections at deep ocean seamounts, Oceanography, 23, 90–103, 2010.

Linke, P. and Lutze, G.: Microhabitat preferences of benthic foraminifera—a static concept or a dynamic adaptation to optimize food acquisition?, Marine micropaleontology, 20, 215–234, 1993.

Marnor, C. et al.: Fan-shaped sponge distribution at DeepInsight Hill from AI-assisted ROV video analysis, manuscript submitted for publication, 2026.

Mashayek, A., Gula, J., Baker, L. E., Naveira Garabato, A. C., Cimoli, L., Riley, J. J., and De Lavergne, C.: On the role of seamounts in upwelling deep-ocean waters through turbulent mixing, Proceedings of the National Academy of Sciences, 121, e2322163 121, 2024.

Meyer, H. K., Davies, A. J., Roberts, E. M., Xavier, J. R., Ribeiro, P., Glenner, H., Birkely, S.-R., and Rapp, H.: Beyond the tip of the seamount: Distinct megabenthic communities found beyond the charismatic summit sponge ground on an arctic seamount (Schulz Bank, Arctic Mid-Ocean Ridge), Deep Sea Research Part I: Oceanographic Research Papers, 191, 103 920, 2023.

https://doi.org/10.5194/egusphere-2026-1261
Preprint. Discussion started: 18 March 2026

Pearson, P. N. and Party, I. E. . S. S.: A deep-sea agglutinated foraminifer tube constructed with planktonic foraminifer shells of a single species, Journal of Micropalaeontology, 37, 97–104, 2018.

Roberts, E. M., Mienis, F., Rapp, H. T., Hanz, U., Meyer, H. K., and Davies, A.: Oceanographic setting and short-timescale environmental variability at an Arctic seamount sponge ground, Deep Sea Research Part I: Oceanographic Research Papers, 138, 98–113, https://doi.org/10.1016/j.dsr.2018.06.007, 2018.

Schönberg, C. H. L.: No taxonomy needed: Sponge functional morphologies inform about environmental conditions, Ecological Indicators, 129, 107 807, https://doi.org/10.1016/j.ecolind.2021.107807, 2021.

Souche, A., Hartz, E. H., Rüpke, L. H., and Schmid, D. W.: Role of Lee Wave Turbulence in the Dispersion of Sediment Plumes, Oceans, 6, 77, https://doi.org/10.3390/oceans6040077, 2025.

van Haren, H., Hanz, U., de Stigter, H., Mienis, F., and Duineveld, G.: Internal wave turbulence at a biologically rich Mid-Atlantic seamount, PLoS One, 12, e0189 720, https://doi.org/10.1371/journal.pone.0189720, 2017.

Voet, G., Quadfasel, D., Mork, K. A., and Søiland, H.: The mid-depth circulation of the Nordic Seas derived from profiling float observations, Tellus A: Dynamic Meteorology and Oceanography, 62, 516–529, https://doi.org/10.1111/j.1600-0870.2010.00444.x, 2010.

Voje, T., Pedersen, R. B., Thorseth, I., Stubseid, H., Jæger, M., Fredriksen, R., Stenløkk, J., Rom, J., Marnor, C., Kulkarni, M., Sørensen, T., Inderberg, S., Skeie, K., Ousdal, I., Thoresen, G., and Sundnes, L.: Cruise Report - DeepInsight2025: KH25-263, Cruise report, Centre for Deep Sea Research, University of Bergen and Norwegian Offshore Directorate, Bergen, Norway, https://www.sodir.no/49954e/globalassets/1-sodir/om-oss/opne-data/havbunnsmineraler-eng/01-kh25-263-cruise-report-public.pdf, part of EMINENT Project, 2025.

Whalen, C. B., De Lavergne, C., Naveira Garabato, A. C., Klymak, J. M., MacKinnon, J. A., and Sheen, K. L.: Internal wave-driven mixing: Governing processes and consequences for climate, Nature Reviews Earth & Environment, 1, 606–621, 2020.

Witte, U., Brattegard, T., Graf, G., and Springer, B.: Particle capture and deposition by deep-sea sponges from the Norwegian-Greenland Sea, Marine Ecology Progress Series, 154, 241–252, 1997.